Transparent, Double-Sided, ITO-Free, Flexible Dye-Sensitized Solar Cells Based on Metal Wire/ZnO Nanowire Arrays

Wei Wang, Qing Zhao, Heng Li, Hongwei Wu, Dechun Zou, and Dapeng Yu**

Transparent, double-sided, flexible, ITO-free dye-sensitized solar cells (DSSCs) are fabricated in a simple, facile, and controllable way. Highly ordered, high-crystal-quality, high-density ZnO nanowire arrays are radially grown on stainless steel, Au, Ag, and Cu microwires, which serve as working electrodes. Pt wires serve as the counter electrodes. Two metal wires are encased in electrolyte between two poly(ethylene terephthalate) (PET) films (or polydimethylsiloxane (PDMS) films) to render the device both flexible and highly transparent. The effect of the dye thickness on the photovoltaic performance of the DSSCs as a function of dye-loading time is investigated systematically. Shorter dye-loading times lead to thinner dye layers and better device performance. A dye-loading time of 20 min results in the best device performance. An oxidation treatment of the metal wires is developed effectively to avoid the galvanic-battery effect found in the experiment, which is crucial for real applications of double-metal-wire DSSC configurations. The device shows very good transparency and can increase sunlight use efficiency through two-sided illumination. The double-wire DSSCs remain stable for a long period of time and can be bent at large angles, up to 107°, reversibly, without any loss of performance. The double-wire-PET, planar solar-cell configuration can be used as window stickers and can be readily realized for large-area-weave roll-to-roll processing.

1. Introduction

Dye-sensitized solar cells (DSSCs) have attracted intensive interest in both academic and industrial fields due to their low cost and high efficiency.[1–3] Planar DSSCs based on indium tin oxide (ITO) and TiO_2 can reach a photovoltaic conversion efficiency of 11.1%.[4–6] Very recently, a photovoltaic conversion efficiency exceeding 12% was achieved in porphyrin-sensitized solar cells with a cobalt (II/III)-based redox electrolyte.[7] However, ITO films need to be deposited with rare and expensive materials, such as indium, and lack flexibility, limiting their development. The development of flexible DSSCs has become popular because of their lightweight, low-cost roll-to-roll mass production, and wide areas of use.[8,9] For example, flexible DSSCs have been fabricated on polymer/ITO/electrode substrates.[10] Nevertheless, the use of an ITO film can limit a device's flexibility because it is brittle. It also reduces in conductivity when bent. Metal sheets, such as steel and titanium, have served as working substrates for the synthesis of flexible DSSCs.[11,12] However, metal substrates are heavy and opaque. Recently, fiber-like DSSCs have opened up potential applications owing to their many advantages, such low cost, independence from ITO, light weight, flexibility, and integration with current textile technology.[13–19] The basic structure of a fiber-like DSSC consists of two metal wires twisted together, in which one core wire (e.g., Ti) coated with active TiO_2 layers serves as the working electrode, and a second metal wire (e.g., Pt) serves as the counter electrode.[14] However, such devices are not encapsulated in a transparent cladding, resulting in an unreliable electric contact between the working and counter electrodes, especially when the wires are bent. In addition, the twisted structure of the two metal wires leads to a large part of the working electrode being not covered by the Pt counter electrode, which limits the triiodide-ion transportation and collection efficiency in DSSCs. Immersing the working electrode with TiO_2 nanotubes and the counter electrode in an electrolyte in a glass tube has been reported.[16] Nevertheless, this design causes the DSSCs to lose their flexibility and is not easy to produce on a large scale.

ZnO, which has a bandgap similar to that of TiO_2, has also been studied extensively as an active material for DSSC production. It has shown a series of advantages over TiO_2, such as ease of crystallization, higher electron mobility, lower combination rate, and an abundance of nanostructures.[20,21] The photoactive

W. Wang, Prof. Q. Zhao, H. Li, Prof. D. Yu
State Key Laboratory for Mesoscopic Physics
and Electron Microscopy Laboratory
School of Physics
Peking University
Beijing 100871, P. R. China
E-mail: zhaoqing@pku.edu.cn; yudp@pku.edu.cn
Dr. H. Wu, Prof. D. Zou
Beijing National Laboratory for Molecular Sciences
Key Laboratory of Polymer Chemistry
and Physics of Ministry of Education
College of Chemistry and Molecular Engineering
Peking University
Beijing 100871, P. R. China

DOI: 10.1002/adfm.201200168

layer, consisting of 1D ordered nanostructures, has the potential to improve the conversion efficiency of DSSCs because it can provide intuitive 1D electric channels and a large internal surface area.[22,23] Here, we report a novel methodology for the fabrication of an extended-area, flexible, transparent, double-sided, substrate-free, planar DSSC, formed with metal wire/ZnO-nanowire arrays as the working electrode and a Pt wire as the counter electrode. Highly ordered, single-crystalline, and high-density ZnO-nanowire arrays were uniformly deposited onto metal microwires. The two metal wires were placed parallel to each other and encapsulated in a poly(ethylene terephthalate) (PET) or polydimethylsiloxane (PDMS) chamber containing the electrolyte (see Experimental Section for the electrolyte used). This system combines several advantages of fiber-like and polymer-based DSSCs and can produce bendable photovoltaics. Because no special substrate was used, the fabricated DSSCs could be very thin and, therefore, lightweight. Light can be introduced from both sides. The ZnO-nanowire arrays were realized readily in various of metal microwires made of Au, Ag, Cu, and stainless steel (Fe for short). The method is cost-effective and it is easy to perform ITO-free roll-to-roll processes.

2. Results and Discussion

Our DSSC fabrication involved several steps. First, highly ordered, very well aligned, high-density ZnO-nanowire arrays were radially uniformly deposited on a 10 cm long, 70 μm-diameter Fe wire via a simple chemical vapor deposition (CVD) method.[24] This wire served as the primary electrode. Note that, in this process, the wire can be very long (up to several tens of centimeters) and a large number of metal wires with highly ordered, uniform ZnO-nanowire arrays can be processed simultaneously to increase the fabrication efficiency. This process is also very easy for scalable mass production. In our previous study, the patterned growth of ZnO-nanowire arrays was realized on a large-scale stainless-steel mesh grid,[24] showing that a large-area, mesh-like, woven solar cell can be produced in a practical manner.[25,26] We also found that method to be very versatile and easily applicable to metal wires of various compositions. We have built ZnO-nanowire arrays on Au, Ag, and Cu microwires (Figure S1, Supporting Information), demonstrating this method's adaptability. Second, a monolayer of dye molecules (N719) was chemisorbed onto the surfaces of the ZnO nanowires. Then, a platinum-wire counter electrode (40 μm) and the ZnO-nanowire-deposited Fe wire were placed in parallel to each other at a distance of 10 μm. They were then encapsulated in between two pieces of PET film. Finally, a liquid electrolyte (see Experimental Section) was introduced into the gaps between the two PET films by capillary action. The resulting DSSC device is illustrated in **Figure 1**. As shown in Figure 1b, it has very good transparency over a large area, and its flat, planar characteristic makes it very attractive for integration with everyday life because it is easy to stick onto transparent planes, such as buildings or car windows, to make use of sunlight. The PET polymer renders our device much more flexible than devices described in previous studies (inset of Figure 1b), which described the encapsulation of two metal wires in glass capillary tubes.[16]

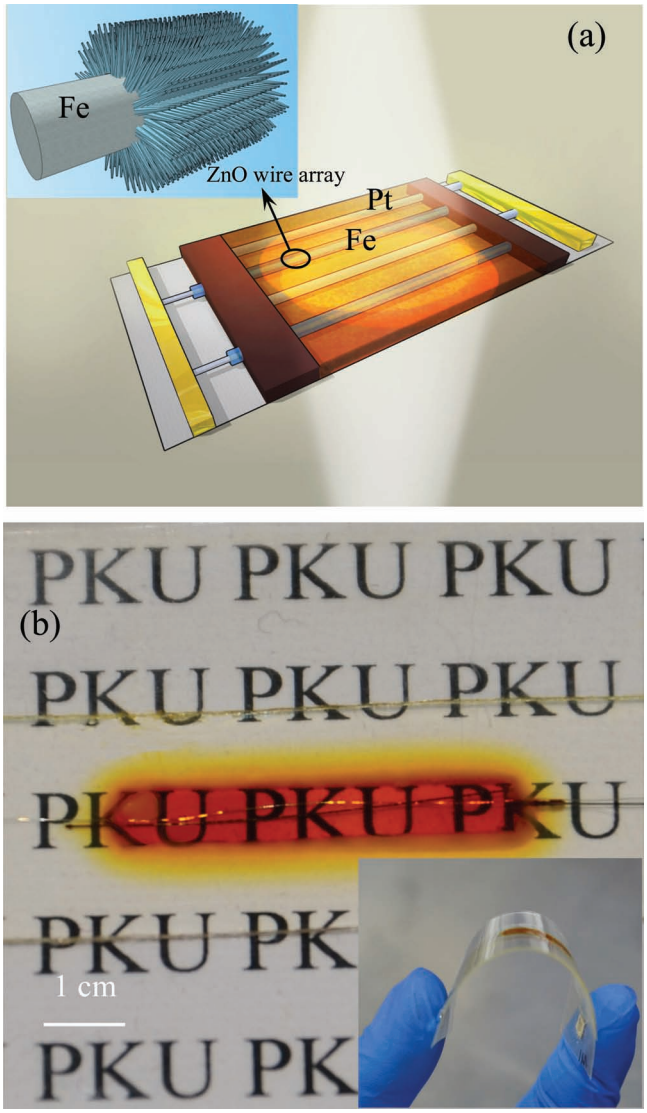

Figure 1. a) Double-metal-wire/PET, double-sided, transparent DSSC device. The Pt acts as the counter electrode. The highly ordered, well-aligned, high-density ZnO-nanowire arrays radially grown on Fe microwire act as working electrodes. The two metal wires were encapsulated in two pieces of PET film. b) The device showed very good transparency. Inset: The device showed very good flexibility with very large bending angle.

The device structure was characterized through scanning electron microscopy (SEM) images. **Figure 2**a shows the typical morphology of the well-aligned, high-density ZnO-nanowire arrays, fully covering the surface of the Fe microwire in a radially outward direction. We could achieve such uniformity along the entire length of the Fe wire easily. From Figure 2b, the Fe microwire was clearly fully and uniformly covered by the highly ordered ZnO-nanowire arrays. ZnO-nanowire arrays with a length of 2 μm and a diameter of 200 nm grew radially on the surface of the Fe wire (Figure 2c,d). The growth density was as high as 5000 mm^{-2}, which could greatly increase the surface area and chemisorption rate of dye molecules. In this way, the concentrically grown ZnO-nanowire arrays were able to block the back electron transfer from the substrate to the electrolyte

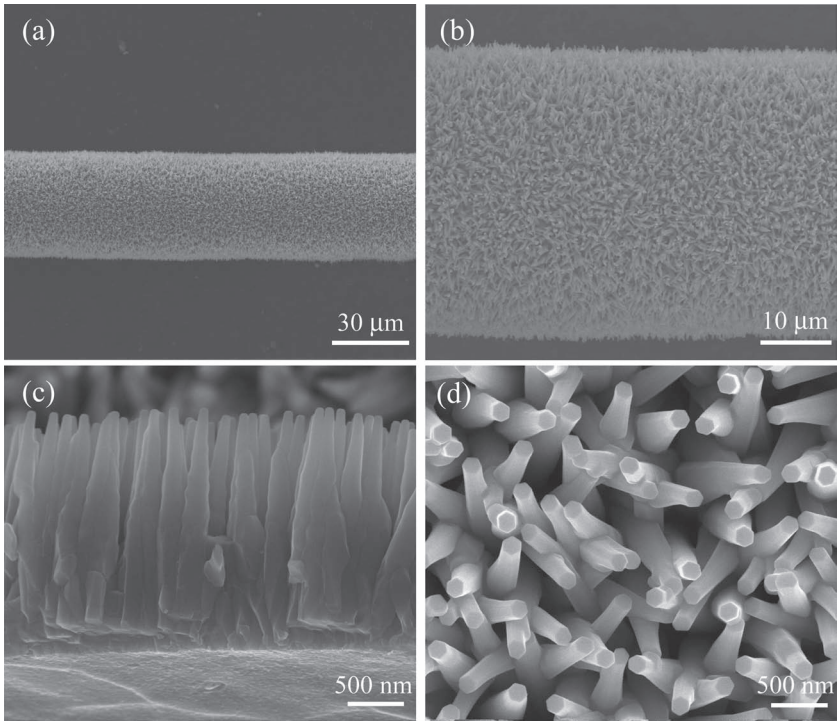

Figure 2. a) SEM image of ZnO nanowire arrays grown on stainless-steel microwires. b) Magnified SEM image of a wire section, uniformly covered with high-density ZnO nanowires. c,d) Cross-section (c) and top-view (d) SEM images showing the well-aligned, high-density ZnO nanowire arrays grown on the stainless-steel microwire.

efficiently, which is vital to suppress the generation of a dark current in the DSCs.[27] Figure 2c shows a dense ZnO buffer layer forming at the interface of the Fe metal and the ZnO-nanowire array during the CVD synthesis. The buffer layer had a flat bottom plane, which helped it adhere to the Fe substrate. This buffer layer could protect the core metal wire from exposure to the electrolyte. Figure 2c also shows that ZnO-nanowire arrays were perpendicular to the Fe wire substrate, which provides undirectional channels for charge transport. This approach could be extended easily to other metal microwires, such as Au, Ag, and Cu. Typical SEM morphologies are shown in Figure S1 (Supporting Information). Compared with conventional TiO_2 nanotubes synthesized through electrochemical anodization, our ZnO nanowires had a much better crystalline quality. This was verified by transmission electron microscopy (TEM). Our nanowires were all single crystalline with very smooth surfaces. This may increase electron diffusion by providing a direct pathway for electron transport from the point of electron injection to the metal wire, because the electrons would not suffer any grain-boundary scattering.[21]

The current density–voltage (J–V) characteristics of the resulting solar cell showed an open-circuit voltage (V_{oc}) of 0.55 V, a short-circuit current (J_{sc}) of 6.42 mA cm^{-2}, and a power conversion efficiency (η) of 0.96% under standard illumination (AM 1.5, 100 mW cm^{-2}) (**Figure 3**a). The effective device area for calculating the efficiency was based on the diameter of the original Fe wire (70 µm) multiplied by the length of wire subjected to illumination (0.5 cm). A more controlled PET-encapsulation process would further improve the performance of our cell devices. One of the most promising advantages of our DSSCs is the flexibility afforded by the polymer materials used to encapsulate the two metal wires. Even under substantial bending (bend 2: radius angle of 107°, winding along the x-direction and bend 3: radius angle of 45°, winding along the y-direction), the V_{oc} (0.19 V), J_{sc} (4.1–4.28 mA cm^{-2}), and cell efficiency (0.21%) remained stable with a strain-free case (Figure 3b). Under the bend-1 condition (radius angle of 55°, winding along the x-direction), the performance of the device was slightly improved, showing an increased V_{oc} of 0.21 V, a J_{sc} of 5.11 mA cm^{-2}, and a cell efficiency of 0.32%. This may be because bending reduces the thickness of the part of the electrolyte facing the light source, thus increasing light transmission. Owing to the high flexibility of the PET film, the DSSC device can be bent at very large angles (107°), unbent, and rebent, without damaging the cell structure, while double-wire, twisted dye-sensitized titania cells will crack with only slight bending.[14] We also extended the cladding material to other transparent polymer materials, such as PDMS, and found it has a good light-conversion efficiency as well (Figure S2, Supporting Information).

The optical properties of the PET film, the electrolyte, and the ZnO-nanowire arrays were examined (**Figure 4**a). The PET showed a light transparency of nearly 100% from 400 to 750 nm. The transmission spectra of the electrolyte indicated a very good transparency (>85%) from 500 to 750 nm, which is the most-active range for the dye molecules, as verified by measurements of the incident-photon-to-electron conversion efficiency (IPCE) (Figure S3, Supporting Information). This indicates that the electrolyte did not affect the light transmission and that light

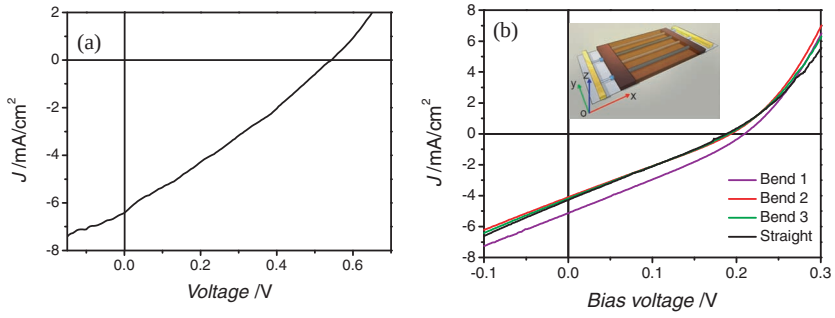

Figure 3. a) J–V characteristics of Fe/ZnO-nanowire-Pt DSSCs in PET film. b) J–V curves of a flexible, planar solar cell in straight form and at bending angles of 55° along the x-direction (Bend 1), 107°, along the x-direction (Bend 2), 45°, along the y-direction (Bend 3), respectively.

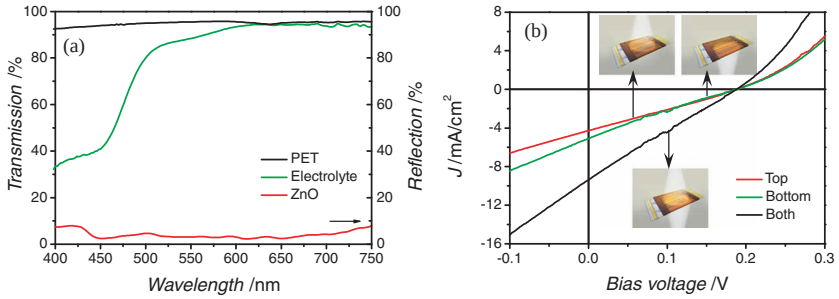

Figure 4. a) Transmission spectra of the PET film and the electrolyte. Reflection spectrum of the ZnO nanowire arrays. b) *J–V* curves of a prototype of a double-sided, transparent DSSC under illumination from the top, bottom, and both sides.

could be effectively absorbed by the dye molecules underneath. The very low reflection over a wide spectrum, 400 to 750 nm, confirmed that the nanowire array structure could trap light and improve light harvesting.[28] The two metal wires were fully immersed in the electrolyte in between two pieces of highly transparent PET film, which allowed the dye molecules on the primary electrode to fully absorb sunlight from all directions and allow uniform illumination over the circumference of the DSSC. The parallel arrangement of the metal wires will also allow the process to be scaled up easily to roll-to-roll large-area mass production using textile technology.

Because the two electrodes were covered with highly transparent PET film, the device had a two-way transparency and could harvest light from both sides (both from the top and the bottom). To confirm this, we measured three typical *J–V* curves of a prototype DSSC, illuminated from above, from below, and from both directions. As shown in Figure 4b, when illuminated from the top or the bottom, a V_{oc} of 0.19 V, a J_{sc} of 4.28 or 5.11 mA cm^{-2}, and a cell efficiency of 0.21% or 0.24% were obtained. When light was illuminated from both the top and bottom, the J_{sc} and the cell efficiency doubled, becoming as high as 9.38 mA cm^{-2} and 0.44%, respectively. These results confirm this type of DSSC is capable of harvesting light from each side to generate electricity, which is significantly more advantageous than using conventional planar solar cells that are opaque on one side. With the flat, planar configuration, these lightweight, planar-type DSSCs can be used as stickers on building windows, where they can utilize light from outside during the day and harvest lamp light from inside at night, nearly doubling the sunlight utilization efficiency.

The amount of dye loaded onto the ZnO nanowire arrays was crucial in determining the conversion efficiency of the DSSCs. Commercially available dyes, such as N719, which is derived from ruthenium polypyridine complexes, have been widely used as sensitizers for TiO_2-based DSSCs, while the effect of N719 absorption to ZnO has not been that widely investigated. It has been found that the surface structure of ZnO crystals may be destroyed after extended exposure to a dye solution.[29] Several studies have reported that a short sensitization time may be favorable to avoid the formation of a Zn^{2+}/dye complex, which is inactive for electron injection.[30,31] Here, we investigated systematically the effects of the dye-loading time on the performance of our solar-cell devices. Low-magnification TEM images indicated that a uniform layer was adsorbed onto the surfaces of the ZnO nanowires (Figure S4a, Supporting Information). Energy-dispersive spectroscopy (EDS) was utilized to verify the existence of a dye-molecule layer on the surface of the ZnO nanowires (Figure S4b, Supporting Information). For different dye-loading times of 10 min, 20 min, and 50 min, the average layer thicknesses outside the ZnO nanowires were determined to be 1.5 ± 0.2 nm, 2.5 ± 0.3 nm, and 5.5 ± 0.2 nm, respectively. Typical TEM images are shown in **Figure 5**a, b, and c, respectively. It has been reported that a Zn^{2+}/dye-complex layer forms on the ZnO-nanostructure surface when lengthening the dye-immersion time.[29] These Zn^{2+}/dye complexes agglomerate to form a thick covering layer instead of a monolayer, and are therefore inactive for electron injection.[21,32] The layer covering outside the ZnO nanowires observed in the TEM images may be these Zn^{2+}/dye-complex agglomerates if the dye-immersion time is long. Longer dye-loading times led to thicker layers, showing a good linear dependence of the layer thickness as a function of loading time over the course of 1 h (Figure 5d). TEM is a powerful technique, suitable to the analysis of dye-loading dynamics in nanostructure-based DSCs.

The J_{sc} was then measured over time for five sections of the same metal wire, which had been covered with layers of different thicknesses, as indicated in the inset of Figure 5e, by using a slit (5 mm), under 1.5 a.m. solar-simulator illumination. The J_{sc} of each section was recorded every 15 s. The J_{sc} decreased as the dye-loading time increased, implying that using a longer dye-immersion time would cause the formation of the Zn^{2+}/dye-complex agglomerate, hindering effective electron injection from the dye molecules to the ZnO.[32] The J_{sc} was found to decrease substantially when light was illuminated on the sections of the working electrode with thicker layers: from 5.39 mA cm^{-2} (20 min dye loading) to 5.16 mA cm^{-2} (30 min dye loading), to 4.62 mA cm^{-2} (40 min dye loading), and to 3.55 mA cm^{-2} (50 min dye loading). The J_{sc} as a function of dye-loading time is summarized in Figure 5d. A dye-loading time of 20 min (2.5 nm layer thickness) was found to produce the highest J_{sc} and cell efficiency (0.35%). Three typical *J–V* curves corresponding to three different layer thicknesses (1.5 nm, 2.5 nm, and 5.5 nm) are shown in Figure 5f. The layer thickness of 2.5 nm showed both the highest J_{sc} and the largest V_{oc}, 0.23 V. These results tell us that a prolonged dye-loading time (>20 min) may worsen the device performance by forming Zn^{2+}/dye-complex agglomerates, which are inactive to electron injection. A very short dye-loading time (<10 min) may result in incomplete dye-molecule absorption onto the ZnO nanowires. Our optimized dye-loading time (20 min) was also much shorter than the conventional 24 h for TiO_2 DSCs. This may increase the efficiency of cell fabrication.

One attractive characteristic of our double-wire DSCs is that the metal core for the ZnO-nanowire-array growth is an extremely effective transporter of photogenerated electrons due to the very high conductivity. This reduces any photocurrent loss during long-distance transport. We verified this by measuring the resistance between the Fe microwire and the ZnO-nanowire array at different positions along the Fe wire. Electrode I made

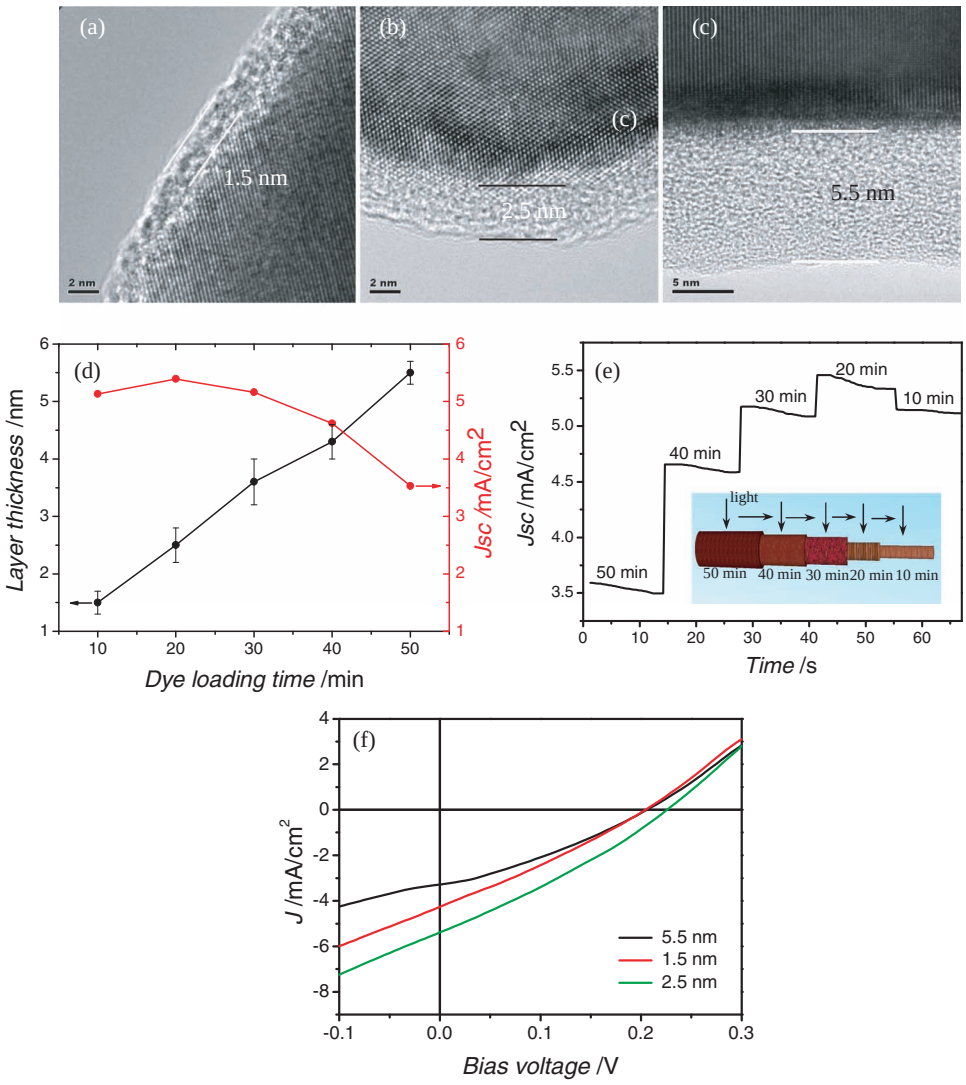

Figure 5. a–c) Typical TEM images of the layer thickness on the surface of ZnO nanowires under different dye loading times: 10 min (a); 20 min (b); 50 min (c). d) Average layer thickness and J_{sc} as a function of dye-loading time. e) J_{sc} of the five sections with different dye-loading times, measured in time order, as indicated in the inset. f) *J*–*V* curves of the samples with layer thicknesses of 1.5 nm (10 min), 2.5 nm (20 min), and 5.5 nm (50 min).

direct contact with the bare Fe wire, and electrodes II, III, and IV made contact with the ZnO-nanowire arrays at intervals of 5 mm to the nearest electrode (Figure S5a, Supporting Information). We measured the resistance at three different positions (electrode II, III, and IV) on the ZnO-nanowire arrays on the Fe wire, with different distances to electrode I. A very low resistance of 500 Ω was detected (Figure S5b, Supporting Information). This indicates that a minimal internal series resistance and effective long-distance charge transport could be achieved in our system. Note that our ZnO nanowires were doped with Al during synthesis in order to increase the carrier concentration. This may facilitate the use of very long metal wires and integration into scalable roll-to-roll processing.

As we mentioned earlier, ZnO nanowires can be deposited readily on microwires made of various metals, such as Au, Ag, Cu, and Fe. DSSCs based on these metal microwires were studied carefully and the performance of Au-based DSSCs was found to be much poorer than those of Ag, Cu, or Fe-based DSCs because of the large Schottky barrier (Figure S6a, Supporting Information). The large work-function discrepancy between the Au (5.1 eV) and the Al-doped ZnO (4.2 eV) made it difficult for an ohmic contact to be formed between the Au and the ZnO (Table S1, Supporting Information). The Schottky barrier decreased the overall performance of the solar cells. When we measured the *J*–*V* curves of DSSCs made on wires not given any prior treatment, a dark-current density of 2.03 mA cm^{-2} was observed when there was no voltage applied and no light illumination (**Figure 6**a). As shown in Figure 6b, there was still a dark current when the light was switched off. All of these results indicate that a galvanic cell may exist in our system. Cracks may be generated between the ZnO buffer layer and metal wires after multiple bending operations and expose the metal microwire core to the electrolyte and to the Pt at the same time. We found such cracks by SEM analysis

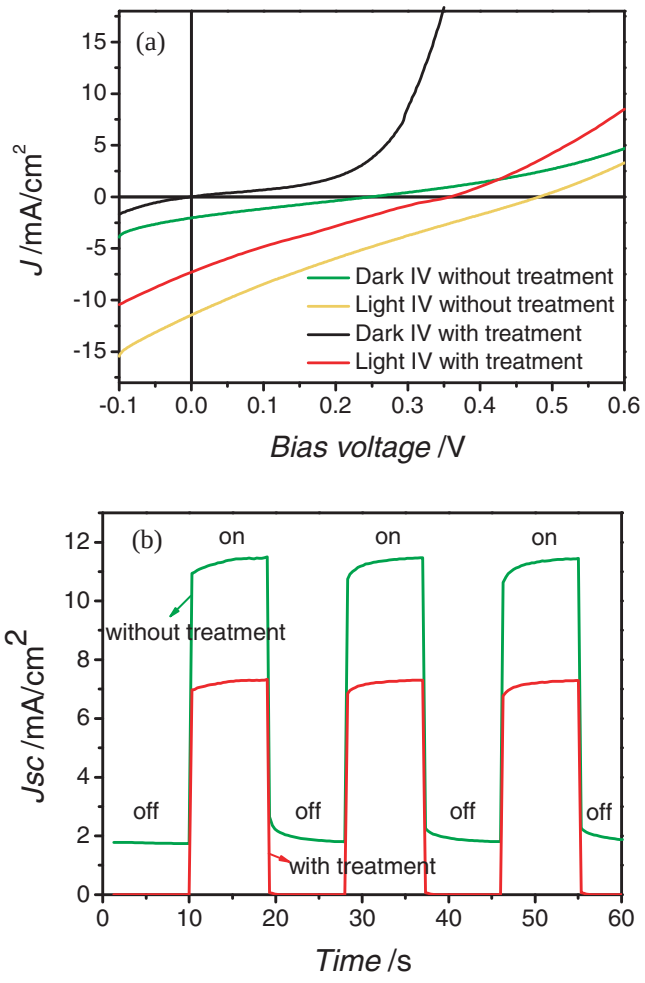

Figure 6. a) Dark and light *J–V* curves of the as-fabricated DSSCs with and without oxidation treatment. b) J_{sc} of the DSSCs with and without oxidation treatment with light on and off.

after we got a nonzero dark current (Figure S6b, Supporting Information). The electric potential between the Pt electrode and other bare metal microwires (without ZnO) was measured by immersing them in the electrolyte. We found a relative reduction potential between them (from 0.035 to 0.832 V (Table S1, Supporting Information)), indicating that a galvanic battery existed between the Pt counter electrode and the metal-core electrode in the electrolyte. This is a very important issue for double-metal-wire-shaped DSSCs, because there is a significant risk that metal cores coated with either TiO_2 or ZnO can be exposed to the electrolyte solution, causing a galvanic-battery reaction. These reactions can eventually cause metal corrosion and render the device non-functional. Ag and Cu showed larger relative reduction potentials than Au and Fe (Table S1, Supporting Information). Because Au can form a Schottky barrier with ZnO, we chose Fe for our later experiments. An effective method of avoiding such reactions is highly desirable in order to maintain the device performance. In order to get rid of the galvanic battery, an oxidizing layer was introduced before the ZnO deposition to protect the metal from the electrolyte. The Fe microwire was immersed in a 4:1 mixture of H_2SO_4 (97%) and H_2O_2 (30%) for 30 min after cleaning with acetone for 15 min. After the treatment, the ZnO nanowire arrays were deposited and the DSSC devices were fabricated. After introducing the oxide layer to the Fe wire, the galvanic-battery effect was effectively suppressed, as verified by the zero dark-current curve at $V = 0$ (Figure 6a). Furthermore, the photoresponse curve, by turning the light on and off, showed that the dark current had been effectively removed (Figure 6b). Except where otherwise noted, all of the data shown in this paper were obtained after introducing an oxide layer onto the Fe microwire. This method provides an effective means of avoiding the galvanic-battery effect in solution, which is very important for making flexible metal-wire-based DSSCs.

We tested the stability of the device over time (**Figure 7**). It has been reported that bare Ti-TiO_2-Pt cells degrade quickly to only 20% of their original efficiency over the course of several minutes because the Pt electrode does not remain immersed in the electrolyte solution during electrolyte vaporization.[33] In contrast, our solar cells showed a very stable performance over 120 min, with an almost-constant J_{sc} of 6.5 mA cm^{-2}. Our double-wire/PET design kept the Pt electrode fully immersed in the electrolyte solution and retained the liquid to maintain long-lasting stability.

The conversion efficiency of our ZnO-nanowire-based DSSCs was not as high as that obtained by using TiO_2 nanotubes. This may be due to the relatively slow electron-injection kinetics from the dye to the ZnO and an imperfect PET-packaging technique. One possible means of improving the performance of our DSSCs would involve the sputtering of a thin layer of Ti onto the surface of the ZnO-nanowire arrays to increase the electron-injection efficiency. The open-circuit voltage was relatively low, which may have been caused by an imperfect contact between the ZnO and the metal, and possible leaking at the interface between the metal wire and the electrolyte. Further work is underway to improve the contact and add a thin coating onto the metal wires to avoid leaking. Carbon materials such as a carbon-nanotube film or graphene may lower the fabrication

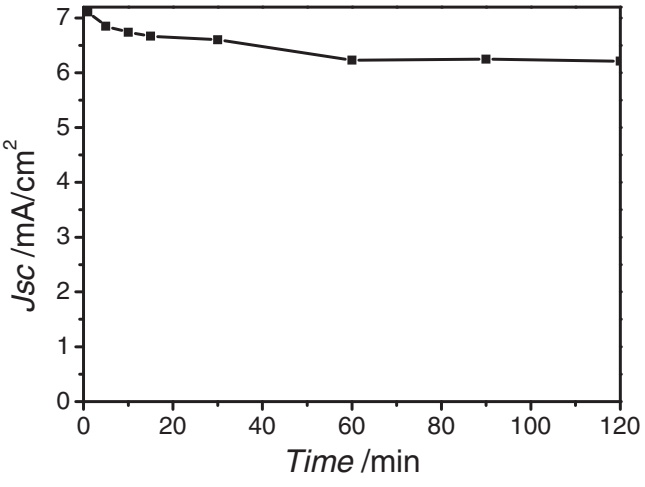

Figure 7. Recorded J_{sc} of a typical as-fabricated DSSC over a period of 120 min.

costs if used as counter electrode materials. The combination of several dye molecules with different absorption bands may enlarge the light-absorption wavelength range of the device.

3. Conclusions

In conclusion, transparent, double-sided, ITO-free, flexible DSCs were developed in a double-metal-wire/PET-film configuration. Metal wires coated with highly ordered ZnO-nanowire arrays acted as working electrodes and Pt wires served as counter electrodes. Because the two wires were immersed in electrolyte between PET films, rather than rigid or opaque substances, the device showed very good flexibility and high transparency. The effect of the dye thickness on the cell performance was studied systematically and an optimized dye-loading time of 20 min was deduced. An effective surface-treatment method was developed to prevent the galvanic-cell effect. The parallel placement of the metal wires may open up possibilities for integration in textile and fabric production for large-area, mesh-like solar cells.

4. Experimental Section

Preparation of ZnO-Nanowire Arrays: Highly oriented ZnO-nanowire arrays were deposited onto an Fe microwire (70 μm, 99.9% in purity) by chemical vapor deposition. Before ZnO deposition, the Fe microwire was immersed in a 4:1 mixture of H_2SO_4 (97%) and H_2O_2 (30%) for 30 min, followed by acetone cleaning for 15 min. This step formed an oxide layer outside the Fe wire to protect the metal core and avoid the galvanic-battery effect, as discussed in the main text. A mixture of Zn powder (0.15 g) and $AlCl_3{\cdot}6H_2O$ powder (0.05 g) in a quartz tube and an Fe microwire 1 cm downstream from the quartz tube were placed in the furnace tube. The tube furnace was heated to 700 °C and the temperature was maintained for 5 min with 100 sccm Ar and 8 sccm O_2 at 1 Pa. Al-doped ZnO-nanowire arrays were synthesized to increase the electron concentration and mobility. ZnO-nanowire arrays were deposited onto Au (45 μm), Ag (25 μm), and Cu (10 μm) wires using the same method.

Fabrication of Solar-Cell Devices: The ZnO-nanowire arrays, radially grown around the Fe wires, were immersed in cis-bis(isothiocyanato) bis(2,2-bipyridyl-4,4-dicarboxylato)ruthenium (II) bistetrabutyl ammonium (N719, Solaronix, 0.5×10^{-3} M) in ethanol (Aldrich) for 20 min at 50 °C, followed by an ethanol rinse to remove any physically adsorbed dye molecules. Then, a platinum-wire counter electrode (d = 40 μm, 99.9% purity) was collocated parallel to the working electrode wire at an approximate distance of 100 μm. These two wires were sandwiched in between two pieces of PET (thickness: 80 μm, 3M) using adhesive tape (300LSE, 3M) to assemble the solar cell. The electrolyte, consisting of lithium iodide (0.5 M, >99.9%, Aldrich), iodine (0.05 M, >99.99%, Aldrich), lithium perchlorate (0.05 M, >99.99%, Aldrich), and 4-tert-butylpyridine (0.5 M, >99%, Aldrich) in acetonitrile (GR, Tjshield) was introduced into the gap between the two PET films by capillary action.

Characterization and Solar-Cell Tests: The morphology of the ZnO-nanowire arrays was characterized using scanning electron microscopy (SEM) (Nano430, FEI). The spectral photoresponse and optical properties were measured using a QTest Station 1000AD system (CrownTech Inc). The photocurrent–voltage (J–V) characteristics were obtained using a Keithley model 4200 source measure unit. The cell was illuminated by solar simulator (SolarIV-150A, Zolix) under AM1.5 irradiation (100 mW cm^{-2}), whose power was calibrated using an NREL-calibrated Si solar cell. The irradiated length of the DSC wires was set at 0.5 cm, which was defined by a photomask with a 0.5 cm-wide slit. The irradiated area of each DSC wire was taken as its irradiated length multiplied by the diameter of the Fe wire, which was taken as the projected area. To realize a double-sided light-illumination J–V measurement, the top of the DSC was illuminated by the solar simulator (SolarIV-150A, Zolix) under AM1.5 irradiation (100 mW cm^{-2}), with irradiation by another solar simulator (Xenon lamp, Oriel 91192) at AM1.5 from the underside of the DSC.

Analysis of Layer Thickness with Respect to Dye-Loading Time: Our experiment was performed on one individual Fe microwire coated with ZnO-nanowire arrays to ensure uniformity. Dye layers of different thicknesses were fractionally precipitated on a single working electrode. Experimentally, an individual Fe microwire, with the ZnO-nanowire arrays, 10 cm in length was immersed into a N719 dye solution in a beaker at 50 °C. After 10 min, part of the solution was pumped out using a syringe to reduce the liquid volume by 5 mm. This left the top 5 mm of wire exposed to air and permitted a dye-loading time of 10 min. After another 10 min, the procedure was repeated to expose another 5 mm of wire to air, giving this part of the wire a dye-loading time of 20 min. This pump step was repeated five times, giving five different dye-loading times along the Fe microwire: 10, 20, 30, 40, and 50 min. Then, the five samples were characterized carefully by transmission electron microscopy (TEM) (Tecnai F30). The average layer thickness of each sample was measured statistically through many (>10) TEM images taken for several different ZnO nanowires on the Fe wire.

Measurement of Resistance: Parts of the Fe wires coated with the ZnO-nanowire arrays were scratched with tweezers to remove the ZnO nanowires and expose parts of the Fe core to air. One Ti/Au (5 nm/50 nm) electrode (electrode I) was deposited onto the bare Fe wire using magneton sputtering, and another Ti/Au (5 nm/50 nm) electrode (electrode II) was deposited on the ZnO-nanowire arrays of the same Fe wire, 1.5 cm from electrode I. Two more electrodes (electrodes III and IV) were deposited 5 mm from electrodes II and III, respectively (Figure S5a, Supporting Information). The resistance between each pair of electrodes was measured using a Keithley model 4200 source measure unit.

Supporting Information

Supporting Information is available from the Wiley Online Library or from the author.

Acknowledgements

This project was financially supported by the National Natural Science Foundation of China (NSFC 50902004, 11023003, 10974003) and National 973 projects (2009CB623703, 2011CB707601, 2012CB933401, MOST) from China's Ministry of Science and Technology. This work was also supported by the Sino-Swiss Science and Technology Cooperation Program (2010DFA01810).

Received: January 18, 2012
Revised: March 9, 2012
Published online: April 12, 2012

[1] B. O'Regan, M. A. Grätzel, *Nature* **1991**, *353*, 737.
[2] D. Kuang, S. Ito, B. Wenger, C. Klein, J.-E. Moser, R. Humphry-Baker, S. M. Zakeeruddin, M. Grätzel, *J. Am. Chem. Soc.* **2006**, *128*, 4146.
[3] S. Ito, S. M. Zakeeruddin, R. Humphry-Baker, P. Liska, R. Charvet, P. Comte, M. K. Nazeeruddin, P. Pechy, M. Takata, H. Miura, S. Uchida, M. Grätzel, *Adv. Mater.* **2006**, *18*, 1202.
[4] M. K. Nazeeruddin, F. De Angelis, S. Fantacci, A. Selloni, G. Viscardi, P. Liska, S. Ito, B. Takeru, M. Grätzel, *J. Am. Chem. Soc.* **2005**, *127*, 16835.
[5] Y. Chiba, A. Islam, Y. Watanabe, R. Komiya, N. Koide, L. Han, *Jpn. J. Appl. Phys.* **2006**, *45*, L638.

[6] F. Gao, Y. Wang, D. Shi, J. Zhang, M. Wang, X. Jing, R. Humphry-Baker, P. Wang, S. M. Zakeeruddin, M. Grätzel, *J. Am. Chem. Soc.* **2008**, *130*, 10720.
[7] A. Yella, H. W. Lee, H. N. Tsao, C. Y. Yi, A. K. Chandiran, M. K. Nazeeruddin, E. Wei-Guang Diau, C. Y. Yeh, S. M Zakeeruddin, M. Grätzel, *Science* **2011**, *334*, 629.
[8] M. Durr, A. Schmid, M. Obermaier, S. Rosselli, A. Yasuda, G. Nelles, *Nat. Mater.* **2005**, *4*, 607.
[9] D. Kuang, J. Brillet, P. Chen, M. Takata, S. Uchida, H. Miura, K. Sumioka, S. M. Zakeeruddin, M. Grätzel, *ACS Nano* **2008**, *2*, 1113.
[10] H. Lindstrom, A. Holmberg, E. Magnusson, S. E. Lindquist, L. Malmqvist, A. Hagfeldt, *Nano Lett.* **2001**, *1*, 97.
[11] M. G. Kang, N. G. Park, K. S. Ryu, S. H. Chang, K. J. Kim, *Sol. Energy Mater. Sol. Cells* **2006**, *90*, 574.
[12] S. Ito, N. Ha, G. Rothenberger, P. Liska, P. Comte, S. M. Zakeeruddin, P. Péchy, M. K. Nazeeruddin, M. Grätzel, *Chem. Commun.* **2006**, 4004.
[13] M. R. Lee, R. D. Eckert, K. Forberich, G. Dennler, C. J. Brabec, R. A. Gaudiana, *Science* **2009**, *324*, 232.
[14] X. Fan, Z. Chu, F. Wang, C. Zhang, L. Chen, Y. Tang, D. Zou, *Adv. Mater.* **2008**, *20*, 592.
[15] S. Huang, Q. Zhang, X. Huang, X. Guo, M. Deng, D. Li, Y. Luo, Q. Shen, T. Toyoda, Q. Meng, *Nanotechnology* **2010**, *21*, 375201.
[16] Z. Liu, M. Misra, *ACS Nano* **2010**, *4*, 2196.
[17] X. Fan, Z. Chu, L. Chen, C. Zhang, F. Wang, Y. Tang, J. Sun, D. Zou, *Appl. Phys. Lett.* **2008**, *92*, 113510.
[18] S. C. Hou, X. Cai, Y. P. Fu, Z. B. Lv, D. Wang, H. W. Wu, C. Zhang, Z. Z. Chu, D. C. Zou, *J. Mater. Chem.* **2011**, *21*, 13776.
[19] D. C. Zou, D. Wang, Z. Z. Chu, Z. B. Lv, X. Fan, *Coord. Chem. Rev.* **2010**, *254*, 1169.
[20] M. Quintana, T. Edvinsson, A. Hagfeldt, G. Boschloo, *J. Phys. Chem. C* **2007**, *111*, 1035.
[21] Q. Zhang, C. S. Dandeneau, X. Zhou, G. Cao, *Adv. Mater.* **2009**, *21*, 4087.
[22] K. Zhu, N. R. Neale, A. Miedaner, A. J. Frank, *Nano Lett.* **2007**, *7*, 69.
[23] J. R. Jennings, A. Ghicov, L. M. Peter, P. Schmuki, A. B. Walker, *J. Am. Chem. Soc.* **2008**, *130*, 13364.
[24] X. Y. Xu, H. Z. Zhang, Q. Zhao, Y. F. Chen, J. Xu, D. P. Yu, *J. Phys. Chem. B* **2005**, *109*, 1699.
[25] X. Fan, F. Z. Wang, Z. Z. Chu, L. Chen, C. Zhang, D. C. Zou, *Appl. Phys. Lett.* **2007**, *90*, 073501.
[26] Z. Y. Liu, V. Subramania, M. Misra, *J. Phys. Chem. C* **2009**, *113*, 14028.
[27] S. Ito, P. Liska, P. Comte, R. Charvet, P. Péchy, U. Bach, L. Schmidt-Mende, S. M. Zakeeruddin, A. Kay, M. K. Nazeeruddin, M. Grätzel, *Chem. Commun.* **2005**, 4351.
[28] C. Battaglia, J. Escarre, K. Söderström, L. Erni, L. Ding, G. Bugnon, A. Billet, M. Boccard, L. Barraud, S. Wolf, F.-J. Haug, M. Despeisse, C. Ballif, *Nano Lett.* **2011**, *11*, 661.
[29] H. Horiuchi, R. Katoh, K. Hara, M. Yanagida, S. Murata, H. Arakawa, M. Tachiya, *J. Phys. Chem. B* **2003**, *107*, 2570.
[30] K. Westermark, H. Rensmo, H. Siegbahn, K. Keis, A. Hagfeldt, L. Ojamae, P. Persson, *J. Phys. Chem. B* **2002**, *106*, 10102.
[31] T. P. Chou, Q. F. Zhang, G. Z. Cao, *J. Phys. Chem. C* **2007**, *111*, 18804.
[32] R. Katoh, A. Furube, Y. Tamaki, T. Yoshihara, M. Murai, K. Hara, S. Murata, H. Arakawa, M. Tachiya, *J. Photochem. Photobiol. A* **2004**, *166*, 69.
[33] S. Zhang, C. Ji, Z. Bian, R. Liu, X. Xia, D. Yun, L. Zhang, C. Huang, A. Cao, *Nano Lett.* **2011**, *11*, 3383.